Photoluminescence properties of the entire excitonic series in Cu_2O

Mitsuyoshi Takahata and Nobuko Naka*

Department of Physics, Kyoto University, Kitashirakawa-Oiwake-cho, Sakyo-ku, Kyoto 606-8502, Japan

(Received 17 July 2018; revised manuscript received 28 September 2018; published 21 November 2018)

We investigated the photoluminescence spectra of Cu_2O under photoexcitation at 3.05 eV across the violet band gap. The following three features were found: photoluminescence from blue and violet excitons; photoluminescence from yellow excitons of s, d, and f states in addition to p states with a quantum number up to ten; and emissions associated with the inelastic collision of the 1s yellow excitons. The first process is relevant for the separation of radiative and nonradiative decay rates. The second process likely indicates radiative enhancement of high Rydberg yellow excitons. The last process verifies up-conversion of 1s yellow paraexcitons into higher Rydberg states, which is a critical factor impeding the realization of a high-density paraexciton gas towards transition to the Bose-Einstein condensation.

DOI: 10.1103/PhysRevB.98.195205

I. INTRODUCTION

Investigating the luminescence properties of solids under weak or strong photoexcitation is of fundamental importance to understand linear or nonlinear relaxation processes of excited states out of equilibrium. In the case of semiconductors, a property of particular interest is near band-gap luminescence, which is often affected by the formation of quasiparticles, i.e., excitons. An exciton is a Coulomb-bound pair of an electron and a hole, that may exhibit a hydrogen-like discrete energy series indexed by the principal quantum number n. In particular, Wannier-Mott excitons of a small Bohr radius, such as those in metal oxides (Cu_2O [1] and ZnO [2]), nitrides (GaN [3] and AlN [4]), and transition-metal dichalcogenides [5] (MoS_2, $MoSe_2$, WS_2, and WSe_2), are stable owing to their high binding energies. As excitons remain stable for a wide range of temperatures in such materials, inelastic scattering due to exciton-exciton collisions [6] plays a significant role in their properties. Examining the exciton-exciton collision processes in two-dimensional semiconductors is also very important as it was recently found to be a dominant mechanism for the depolarization of valley degrees of freedom [7].

Despite its significance and the interest it has received, a detailed study of collisional mechanisms in atomically thin layered semiconductors is not straightforward because unwanted extrinsic effects, such as inhomogeneous broadening and interaction with substrates, are related to the preparation method and sample quality. In addition, there are few reports on the relaxation between excited ($n > 2$) and ground ($n = 1$) states of the Wannier exciton series, although many reports have been published on the dynamics of the ground states. Some limited examples are the photoluminescence (PL) studies on CdS [8], β-ZnP_2 [9], CuCl [10], ZnO [11], and Cu_2O [12]. Relaxation between different excitonic series is even less studied [13]. As Cu_2O has the highest excited state ($n = 7$) that has been reported so far in PL [14], it is one of the ideal materials for studying intra- and interseries relaxations of excitons. This material was originally considered for use as a p-type semiconductor in the 1950s, and it is known as the first material in which the Wannier series excitons were experimentally observed in 1952 [15].

Figure 1(a) schematically presents the band structure of Cu_2O near the center of the Brillouin zone. The combination of the two conduction and two valence bands comprises four Wannier series, referred to as the yellow, green, blue, and violet excitons. The band structure of Cu_2O is exceptional in the sense that the spin-orbit interaction is negative for the valence band originating from the copper 3d orbital, and the lowest conduction band originates from the copper 4s orbital. Thus, both the lowest conduction and the highest valence (split-off hole) bands, relevant to the formation of the yellow exciton series, have the same parity. This means that the optical dipole transition to the lowest-energy excitons across this yellow gap is forbidden. As shown in Fig. 1(a), the 1s state of the yellow excitons is further split by an exchange interaction into ortho- and paraexcitons. The paraexcitons have a lifetime in the submicrosecond range, which has motivated many attempts to realize an excitonic Bose condensate [16,17].

In 2014, an epochal report [18] on the observation of giant Rydberg states of the yellow excitons triggered the opening of a new branch of physics on Rydberg excitons. Rapid progress has been made both theoretically and experimentally on the external perturbation on the Rydberg states [19–23], quantum chaos [24], quantum coherence [25], and so on. We recently revisited the PL properties of yellow excitons in Cu_2O and demonstrated that a Rydberg series up to $n = 7$ was observed in PL (i.e., two additional p states in comparison to the previous work by Compaan and Cummins [12]). We proposed that the yellow Rydberg states are likely to be formed by exciton-exciton collision of the 1s paraexctions. Therefore, the luminescence properties of the high Rydberg states could provide insight into the annihilation process of paraexcitons relevant to the Bose condensation.

In this paper, we present a detailed PL study of Cu_2O under excitation across the violet band gap by using the highest

*naka@scphys.kyoto-u.ac.jp

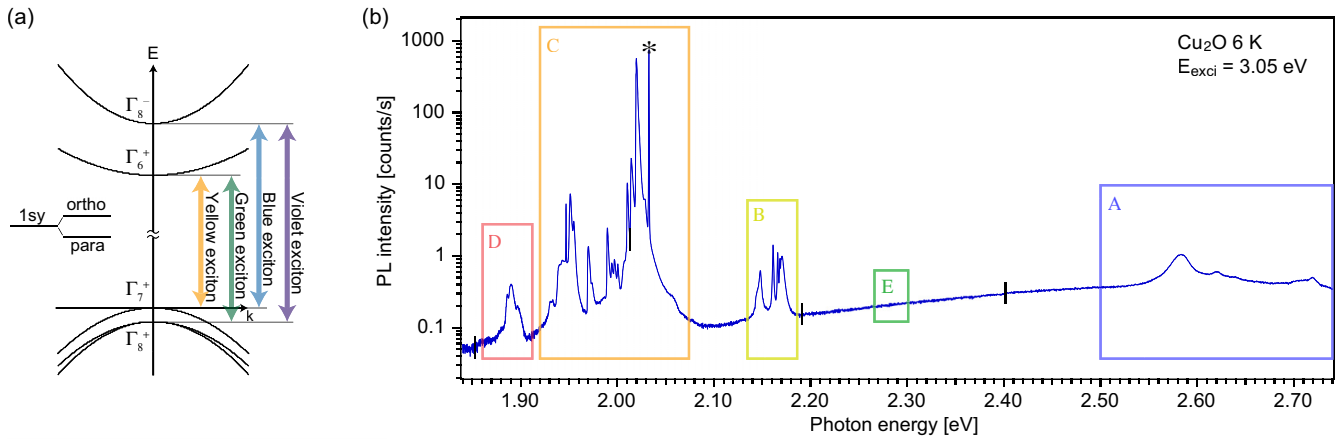

FIG. 1. (a) Schematic of the band structure and excitonic series of Cu_2O. (b) PL spectrum of Cu_2O at 6 K. A: blue and violet excitons; B: yellow excitons with $n \geqslant 2$; C: direct and phonon-assisted transitions of 1*s* yellow excitons; D: emissions associated with up-conversion of the 1*s* yellow exciton; and E: region of the green excitons expected from absorption peaks.

photon energy ever used for the photoexcitation of bulk Cu_2O in previous reports. This enables observations of the blue and violet excitons in the PL spectra, the Rydberg states of the yellow excitons, as well as an investigation of inter- and intraexciton series relaxations. Compared to yellow excitons, blue and violet excitons have not been studied extensively. Table I summarizes some relevant parameters clarified by methods other than PL, i.e., absorption [26], electroreflectance [27,28], and second-harmonic [29] experiments on blue and violet excitons. Many important parameters determining the optical properties of the excitons, such as the nonradiative rates and temperature shifts of the gaps, are also still unknown.

In the following sections, we present the blue and violet excitons observed in the PL spectra. The results provide information on the radiative and nonradiative rates (Sec. III A) and an unambiguous determination of the gap shift as a function of temperature (Sec. III C), which was found to be consistent with the well-known shifts of the yellow and green gaps. Furthermore, the newly found higher yellow Rydberg states in PL, including even-parity (s, d) states and high angular momentum (f) states (Sec. III B) as well as emissions associated with up-conversion of the 1*s* state to higher states of yellow excitons (Sec. III D), will be discussed based on our refined spectra for the yellow excitons.

II. EXPERIMENTS

Thin Cu_2O slabs (thicknesses of ∼1 mm) were cut from a natural crystal, mechanically polished, and then chemically etched by immersion in HCl (2 mol/l) for 10 s and in aqueous NH_3 (13 mol/l) for 10 s to remove the surface defects. Care was taken to avoid deposition of metallic copper on the surfaces. The mother crystal was a high-quality natural Cu_2O in which a 600-ns lifetime was confirmed for the 1*s* yellow paraexciton [30]. The sample was mounted in a closed-cycle cryostat (Pascal, PRDK-205LAVP). The temperature of the cold finger was measured by a silicon diode sensor with an accuracy of ±0.2 K and controlled by a heater in the range of 6–100 K.

The excitation source was a laser diode (Thorlabs, LD5146-101S) at the photon energy of 3.05 eV (407 nm) passed through a bandpass filter (Thorlabs, FBH405-10) for spectral cleaning. The light beam was focused on the sample surface only in the horizontal direction by a combination of a cylindrical lens and a planoconvex lens. The line focusing enabled weak excitation whereas the good signal-to-noise (S/N) ratio was maintained owing to the signal integration along the monochromator slit. After the PL signal was passed through an edge-pass filter (Thorlabs, FELH0450) to cut off the laser scattering light, it was detected by a Peltier cooled charge-coupled-device (CCD) camera after dispersion by a spectrometer (Horiba Jobin Yvon iHR550 or Jobin Yvon THR1500). Long exposure times of the CCD camera over 8 h were adopted to detect very weak PL signals, including those from dipole-forbidden transitions.

The techniques used in this paper, such as chemical etching, line focusing, and the use of high-dispersion monochromators, enabled the discovery of PL lines as will be presented below, which was not possible in our previous study [14].

III. RESULTS AND DISCUSSION

Figure 1(b) shows a PL spectrum measured at 6 K for the entire spectral range from the violet to the yellow excitons. Three spectra taken with various center-wavelength settings of the monochromator (iHR550) were carefully connected without correction for the camera sensitivity and grating diffraction efficiency depending on the wavelength. The connected energy positions are indicated by vertical lines. It should be noted that the strongest line (marked by the asterisk symbol in Box C) is very weak in a general sense because it originates from the dipole-forbidden and quadrupole-allowed transition of the 1*s* orthoexcitons and other lines are much weaker. A high dynamic range exceeding 10^4 was achieved by more than 100 times accumulation of the 16-bit counts.

The PL spectral peaks are categorized into four groups: (A) blue and violet excitons, (B) yellow Rydberg excitons, (C) yellow 1*s* excitons and their phonon replicas, and (D) emissions associated with up-conversion of the 1*s* yellow excitons (according to our interpretation). Among these, group C peaks have been known to exist since the 1960s owing to several studies of Raman processes in Cu_2O [31,32]. Group

TABLE I. Parameters of the blue and violet excitons in Cu_2O. Values from the literature [26,27] are compared with those obtained in our present paper. All values are given in units of eV except for the nondimensional oscillator strengths f.

	Previous paper	Present paper
Exciton energy		
1s blue	2.58 [26], 2.569 [27]	2.5829 ± 0.0001
2s blue	2.62 [26], 2.611 [27]	2.6209 ± 0.0001
1s violet	2.71 [26], 2.693 [27]	2.7191 ± 0.0001
2s violet	2.74 [26], 2.740 [27]	
Energy gap		
Blue	2.63 [26], 2.625 [27]	2.6336 ± 0.0003
Violet	2.75 [26], 2.756 [27]	
Rydberg energy		
Blue	0.053 [26], 0.056 [27]	0.0507 ± 0.0002
Violet	0.040 [26], 0.063 [27]	
Oscillator strength or total width *		
1s blue	5.8×10^{-3} [27]	0.0239 ± 0.0005*
2s blue	6.9×10^{-3} [27]	0.0201 ± 0.0005*
1s violet	9.2×10^{-3} [27]	0.0099 ± 0.0005*

B peaks were reported in our recent paper [14], but in this paper, we obtained even higher Rydberg states: s, d, f, and $n = 8$–10 p states. Attributions of group A and group D peaks will be reported in the following subsections. In the range of Box E, no peaks were found around the energy positions of the absorption peaks for green excitons [33], which implies that the relaxation of holes in the valence band is excessively fast, allowing for the dipole-allowed violet excitons, rather than the green excitons of the (first-class) dipole-forbidden character, to appear in the PL.

In what follows, we discuss the peaks in groups A, B, and D in detail to clarify the mechanism of the processes and derive the relevant parameters.

A. Photoluminescence due to blue and violet excitons and their radiative rates

The enlarged spectrum of group A peaks is shown in Fig. 2(a). The $1s$ and $2s$ excitons of the blue series and the $1s$ violet exciton were resolved. The small bump at 2.743 eV may be a trace of the $2s$ violet exciton, but it is not certain owing to truncation of the signal by the edge-pass filter. The moment analysis of the spectral shape of the $1s$ blue exciton line indicates that the peak is described better by Lorentzian than by Gaussian functions with a kurtosis close to 1.75 for an ideal Lorentzian [14]. Therefore, we fitted the observed spectrum with the sum of three Lorentzian peaks centered at the resonance energies varied as fitting parameters. The agreement between the fit and the data was good. The energy positions obtained for the blue and violet excitons are summarized in Table I, and they are in good agreement with the previously reported positions determined by absorption [26], electroreflectance [27,28], or second-harmonic spectroscopy [29]. The separation (38 meV) of the blue $1s$ and $2s$ excitons indicates a Rydberg energy of $R_{\mathrm{blue}} = 51$ meV and an energy gap of $E_{\mathrm{blue}} = 2.634$ eV in reasonable agreement with previous reports. When the fit function and the data are compared closely, there seems to be an additional component above 2.63 eV in the data. This is probably due to band-edge emission from the continuum states.

We found that these PL signals are observed in samples only with smooth surfaces after fine polishing and chemical treatments. The very weak signals (less than $1/1000$ of the $1s$ quadrupole line even after enhancement by surface treatment) must be the main reason why these PL peaks have not been previously reported. The importance of the surface condition

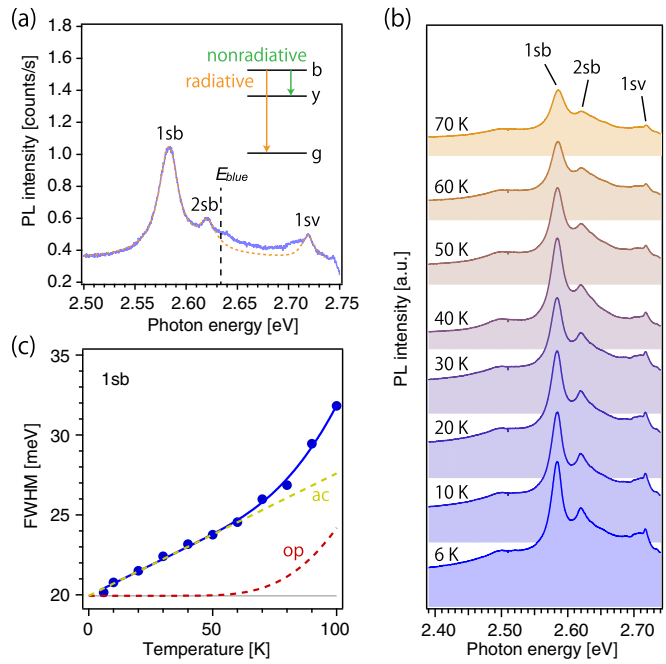

FIG. 2. (a) PL spectrum of blue and violet excitons at 6 K. The dashed line represents the best-fit function. The inset is a schematic of the radiative and nonradiative processes of the blue exciton. (b) PL spectra taken at various temperatures. (c) Temperature dependence of the full width at half maximum (FWHM) of the $1s$ blue exciton line. The solid line represents the fitting result obtained by using Eq. (3).

is highlighted by the fact that the penetration depth of the incident light is as short as 0.04 μm [34].

Our observation of the 1s and 2s blue exciton peaks in the PL led to the extraction of the radiative widths, by assuming that the oscillator strengths follow the relation $f_n \propto 1/n^3$, which is derived from hydrogenlike wave functions [18,35]. It should be noted that the spectrally integrated absorption coefficient is proportional to the radiative rate γ_r, whereas the PL intensity is proportional to $\gamma_r/(\gamma_r + \gamma_{nr})$ [36] where the denominator includes the nonradiative rate γ_{nr}, which leads to the broadening of the line. In Fig. 1(b), it is immediately clear that the PL peaks for blue excitons are much wider than those for yellow excitons. The total linewidths (the FWHM values) are $\hbar\gamma_{tot}^{1sb} = 23.9$ meV for the 1s and $\hbar\gamma_{tot}^{2sb} = 20.1$ meV for the 2s blue exciton. As the conduction band related to the blue excitons is higher in energy than the lowest conduction band by approximately 450 meV [see Fig. 1(a)], the rate for the relaxation of the blue excitons to the lower exciton series should be very high. Here, by considering the small energy separation between the 1s and the 2s blue excitons (38 meV) compared to the separation to other exciton series, we assume that the nonradiative relaxation rate is common for the 1s and 2s blue excitons. By solving the relations,

$$\gamma_{tot}^{1sb} = \gamma_r^{1sb} + \gamma_{nr}^{b}, \tag{1}$$

and

$$\gamma_{tot}^{2sb} = \gamma_r^{2sb} + \gamma_{nr}^{b}, \tag{2}$$

with an assumption that $\gamma_r^{2sb} = \gamma_r^{1sb}/8$, we obtained $\hbar\gamma_r^{1sb} = 4.3 \pm 0.6$, $\hbar\gamma_r^{2sb} = 0.54 \pm 0.08$, and $\hbar\gamma_{nr}^{b} = 19.6 \pm 0.6$ meV.

The results mean that the decay processes of the blue excitons are dominated by nonradiative relaxation because of the existence of lower-lying states. The radiative widths are one order of magnitude smaller than the nonradiative width. This situation differs from the case of the yellow series for which the radiative width is extremely narrow ($\hbar\gamma_r^{2py} = 80$ neV for the 2p state) and many orders of magnitude smaller than the nonradiative width of 3.5 meV [37]. The ratio of the radiative rates for the yellow and blue excitons does not necessarily match the ratio of their oscillator strengths $f_{1sb} = 6 \times 10^{-3}$ for the 1s blue exciton and $f_{2py} = 3 \times 10^{-6}$ for the 2p yellow exciton. The expression for γ_r includes the square of the resonance frequency and the coherence volume [35,37]. The value of γ_r/f was higher for the blue exciton than for the yellow exciton by a factor of 28. This means that, in addition to the larger resonance frequencies, the coherence volume of the blue exciton is larger than that for the yellow exciton. This may be reasonable considering that the polariton effect is much larger for the blue exciton.

In previous studies [27,28] performed only at temperatures of 4, 77 K, or higher, it was difficult to examine temperature dependence due to thermal broadening. In contrast, our clear observation of the Lorentzian peaks for the 1s and 2s blue and 1s violet excitons enabled us also to study the temperature dependence of the relaxation process. Figure 2(b) shows the PL spectra that we obtained at various lattice temperatures from 6 to 70 K. Above this temperature, the peaks are further broadened, and resolving the 2s peak becomes difficult. A fitting analysis similar to the case of Fig. 2(a) was performed to extract the peak positions and the linewidth of the blue and violet excitons. In addition, a small bump was found above 2.48 eV for all the temperatures measured. The bump is likely to be due to two-phonon-assisted transition involving the phonon with Γ_2^- symmetry based on the energy position. This process holds the symmetry requirement for a dipole transition for the exciton state of Γ_4^- symmetry, that is, $\Gamma_4^- \otimes \Gamma_2^- \otimes \Gamma_2^-$, which includes the symmetry Γ_4^- for a dipole operator. The energy of the Γ_2^- phonon decreases by 30% at the X point from the value (43 meV) at the Γ point [38,39]. This explains the plateaulike spectral shape. Additionally, among the 18 phonon modes in Cu_2O, the triply degenerate Γ_5^+ phonon is the only mode with positive parity, allowing for a dipole transition of Γ_4^- excitons by a one-phonon-assisted process. The energy of the Γ_5^+ phonon is 63.8 meV, and the phonon-assisted luminescence can be superimposed on the plateau of the two-phonon-assisted ($2 \times \Gamma_2^-$) luminescence.

Figure 2(c) shows the FWHM of the 1s blue peak as a function of temperature T. The temperature variation of the width can be attributed to the change in the nonradiative rate. We fitted the data with a well-established expression [40,41],

$$\hbar\gamma_{tot} = \hbar\gamma_0 + d_{ac}T + \frac{d_{op}}{\exp(\hbar\omega_{op}/k_BT) - 1}, \tag{3}$$

where the first term includes the radiative and inhomogeneous widths. The third (fourth) term represents intraband scattering by acoustic (optical) phonons with $\hbar\omega_{op}$ being the energy of an optical phonon. The best fit is shown by the solid line, which is in excellent agreement with the data points. We obtained the following values as the fitting parameters: $\hbar\gamma_0 = 19.9 \pm 0.1$ meV, $d_{ac} = 77 \pm 4$ μeV/K, $d_{op} = 660 \pm 50$ meV, and $\hbar\omega_{op} = 43$ meV. The last result indicates an association of the phonon of Γ_2^- symmetry, in accordance with the observation of the two-phonon-assisted process of the same phonon mode in the PL spectra. The obtained values of d_{ac} and d_{op} are both of reasonable magnitude considering those determined in other semiconductors, such as GaAs [42] and ZnSe [43].

The temperature shifts of the blue and violet energy gaps were small and in the opposite direction in energy in comparison to those of the yellow and green energy gaps. This will be discussed in detail in Sec. III C.

B. Yellow Rydberg excitons: f states and higher Rydberg p states

An enlarged spectrum for the yellow excitons in Rydberg states is represented by the solid line in Fig. 3(a). A similar spectrum was already reported in Ref. [14], but here we perform a more detailed analysis, clarifying the additionally higher Rydberg states with n up to ten and other interesting features. As mentioned in Sec. II, this improvement on our previous study [14] is enabled by chemical etching, line focusing, and the use of high-dispersion monochromators.

If the spectral shape of the 3p line in Fig. 3(a) is compared with a Lorentz function (the dotted line), there are two extra components on both side tails. Based on the energy positions of the peaks, these are attributed to even-parity states. In Cu_2O, the d-like term in the effective mass Hamiltonian does

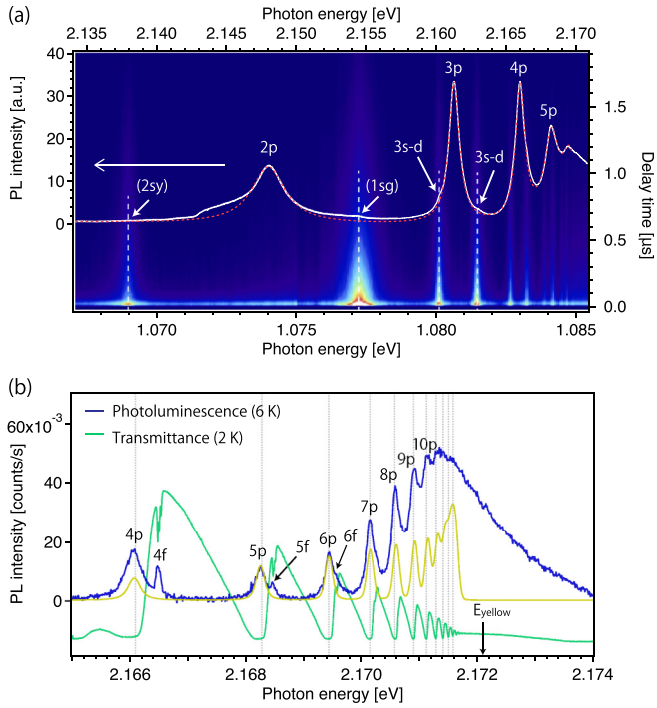

FIG. 3. (a) PL spectrum of yellow excitons in Cu_2O at 6 K (the white line with the upper axis). The contour plot is the signal intensity of the cyclotron resonance of holes under two-photon excitation measured with another sample at 10 K. The horizontal axis represents the photon energy of the excitation light, and the vertical axis is the delay time after pulsed photoexcitation. The data are reproduced from Ref. [45]. (b) Comparison of the PL and transmission spectra of yellow Rydberg states indicating the appearance of f states. The transmission spectrum is shifted by -0.1 meV to correct the temperature shift of the peaks. The yellow line is a simulated spectrum discussed in the text.

not commute with angular momentum L, and this leads to mixing of $L = 0$ (s orbital) and $L = 2$ (d orbital) states [44]. Therefore, we denoted these peaks by $3s$-d. For a direct confirmation, we superimposed the contour plot of a two-photon excitation spectrum for even-parity excitons in Fig. 3(a), which was obtained by scanning the laser wavelength for the cyclotron resonance of holes under two-photon excitation (the plot is reproduced from Ref. [45]). The energy positions showed good agreement. Both these peaks are dipole allowed for a two-photon transition, whereas they are dipole forbidden for one-photon transition and, thus, are very weak in PL.

Figure 3(b) shows a further expanded PL spectrum for the states with $n \geqslant 4$. This high-resolution spectrum was obtained by using a monochromator (THR1500) of a longer focal length (1500 mm) with a 2400-lines/mm grating. The PL spectrum (the blue line) was compared with the transmission spectrum (the green line) through a 210-μm-thick sample, which was cut and prepared from the same mother crystal. In the transmission spectrum, the spectral resolution was further improved to 11 μeV by setting the monochromator to the double-pass configuration and the slit width to 15 μm. The dips for np states were saturated owing to the large thickness of the sample, whereas the dipole-forbidden lines due to high angular momentum states ($4f$-$6f$ excitons) are well resolved.

Unfortunately, the triplet splitting of the f states [46] as seen in the transmission spectrum was not resolved in our PL spectrum owing to the limited spectral resolution for detection of the very weak signal. Nevertheless, the PL linewidth was much narrower for the f states than for the p states, indicating that the optical transitions to the high angular momentum states are only weakly allowed owing to mixing with p states due to the cubic crystal symmetry. It is surprising that the PL intensity is rather high. This indicates that the nonradiative rate for the f states is very small and a large population is accumulated in these long-lived states.

The yellow line in Fig. 3(b) represents an expected PL spectral shape for the $4p$-$14p$ states. We neglected the contributions from f states (which are sufficiently small) and reproduced the spectrum with the sum of Lorentz functions with the total linewidth changing as $1/n^3$ [18,35]. The spectral function was further convolved with a Gaussian to take account of the effective spectral resolution of 100 μeV. The p states with n up to ten are clearly resolved in the experimental data. The actual PL spectrum has an extra component around the energy gap. This enhanced luminescence might be related to the enhancement of the matrix element for the dipole transition owing to the breakdown of the long-wavelength approximation for the extended center-of-mass wave function [47] or to the enhancement of the radiative rates owing to increased coherence length [35].

To conclude this subsection, we observed all the s, p, d, and f states including even-parity ones in the PL of yellow excitonic series.

C. Temperature shift of the violet, blue, green, and yellow gaps

Figure 4(a) shows the PL spectra of yellow Rydberg excitons at various temperatures. Note that the excitation wavelength was different from that for Fig. 2 of Ref. [14]. In addition to the peaks due to np ($n \geqslant 2$) excitons, we found a small peak between the $2p$ and the $3p$ lines as indicated by the solid triangles. The energy position agrees with that of the peak in the two-photon excitation spectrum shown in Fig. 3(a), which was originally attributed to the $2s$ yellow exciton but recently has been reattributed to the $1s$ green exciton [48]. A small edge is also seen below the $2p$ peak as indicated by the open triangles. Based on the spectral shape, this structure seems to be a phonon-assisted transition. The energy separation to the above-mentioned peak is 11.5 meV, and that to the $3s$-d peak in the low-energy tail of the $3p$ peak is 17.3 meV. The position is a little too far (close) to be considered the Γ_5^- (Γ_4^-) phonon replica (see the Appendix for the phonon energies). Attribution of this edge based on the temperature shift of the green/yellow gap will be a future task [49].

The temperature dependence of the position of the $3p$ yellow exciton is presented in Fig. 4(b). The data points for the $1s$ blue and $1s$ violet excitons, obtained through the analysis explained in Sec. III A, are also plotted. As previously mentioned, the temperature shifts of the blue and violet excitons are towards the higher-energy side when the temperature increases. On the other hand, yellow excitons redshifted with increasing temperature. Referring to Fig. 1(a), the respective conduction bands are shared between the violet and the blue

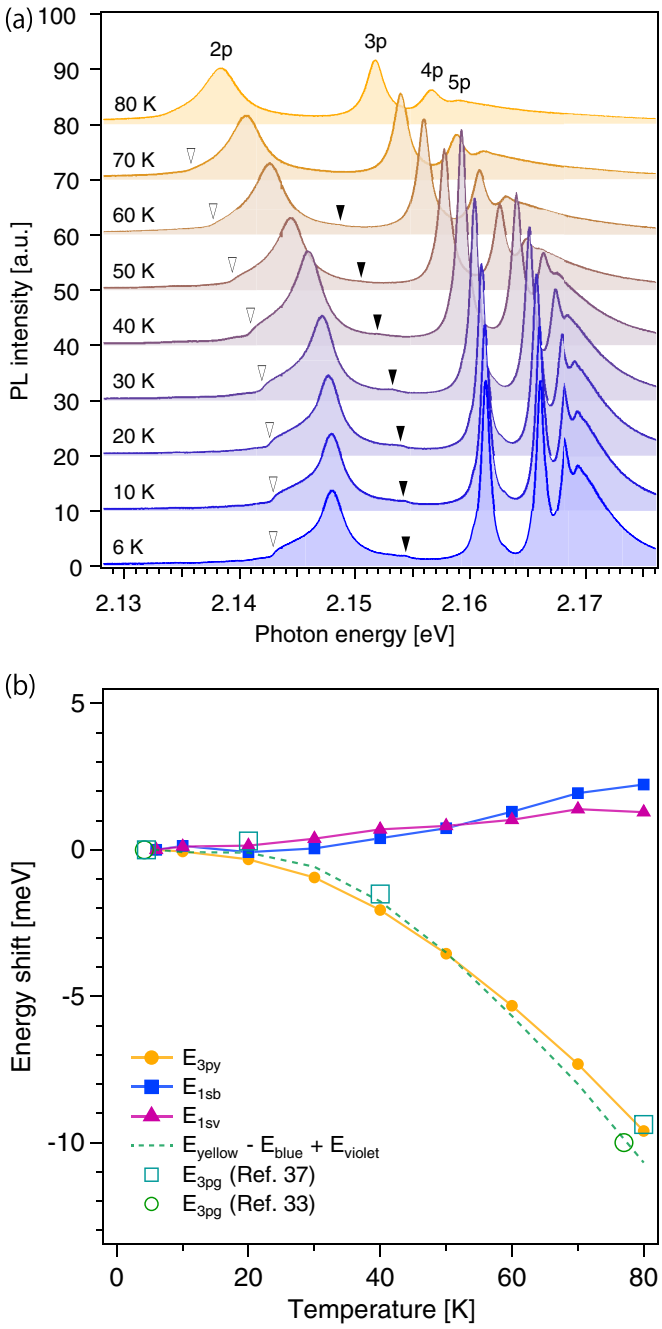

FIG. 4. (a) PL spectra of yellow excitons at various temperatures under excitation at 3.05 eV. The structures indicated by open and solid triangles are discussed in the text. (b) Energy shift of the exciton peaks as a function of temperature.

or the green and the yellow excitons, whereas the respective valence bands are shared between the yellow and the blue or the green and the violet excitons. This means that the temperature variation of $E_{\text{yellow}} - E_{\text{blue}}$ should agree with that of $E_{\text{green}} - E_{\text{violet}}$. Therefore, we calculated $E_{\text{yellow}} - E_{\text{blue}} + E_{\text{violet}}$ based on the measured positions in PL, which serves as a prediction for the temperature variation of the green gap E_{green}. The predicted variation is indicated by the dashed line in Fig. 4(b).

As no PL was observed in the region of green excitons [see Box E in Fig. 1(b)], we plotted the energy shift of the $3p$ green exciton observed by absorption in a thin film [37] by open squares. The agreement of the data with the prediction of E_{green} is convincing, including the slight blueshift of the violet and green gaps in the intermediate-temperature range (20–50 K). For further confirmation, we also plotted previously reported values of the $3p$ green peak measured by absorption on a thin slab [33].

D. Emissions associated with up-conversion from the 1*s* to the Rydberg yellow excitons

In this subsection, we discuss the origin of group D peaks. The emission lines appear approximately at an energy lower by the amount of the exciton binding energy E_x than the $1s$ energy. A detailed understanding of the origin of this group of peaks is important because it can provide insight into how the PL from high Rydberg yellow p states appears although their energy relaxation after photoexcitation is expected to be very fast.

Under intense photoexcitation, interactions between two excitons can manifest themselves in PL spectra. In a wide range of materials [50], two excitons can fuse into an excitonic molecule, leading to a luminescence peak called the M line. Owing to the balance between the electron and the hole effective masses, formation of excitonic molecules is unstable in Cu_2O. Another feature known as P lines or P-band emission was first observed in CdS [51] and attributed to inelastic collisions between two excitons. Instead of fusing into an excitonic molecule, a part of the energy of one exciton is delivered to the other by emission of a photon. The P-band emission is distinguished from the Auger process [52] in which all the energy of one colliding exciton is delivered to the other.

Figure 5(a) schematically shows the P-band emission process associated with the collision of two $1s$ excitons, initially populated at an energy E_{init}. After the collision, one exciton is transferred to a higher-energy (np) state at E_{final}, whereas the other one radiatively recombines by emitting a photon with an energy equal to $E_P = 2E_{\text{init}} - E_{\text{final}} = E_{\text{yellow}} - 2E_x + R_y/n^2 - \Delta$ $(n = 2, 3, \ldots, \infty)$. Here, R_y is the Rydberg energy, and Δ is a positive quantity depending on the difference in the kinetic energies of the initial and final states. The momentum is also conserved by satisfying the relation $2k_{\text{ini}} = k_{\text{final}} + E_P/(\hbar v)$, where v is the speed of light in the medium. The calculated energies E_P with $\Delta = 0$ are indicated by vertical bars at the bottom of Fig. 5(b). The strongest peak within Box D energetically matches with the P line associated with up-conversion from $1s$ paraexcitons to $2p$ excitons. Other smaller peaks also coincide with the expected positions for para-para-collision to the $3p$ state or ortho-para-collision to the $2p$ and $3p$ states.

As the P-band emission is a two-body exciton process, a quadratic dependence on the excitation power is strong proof. To confirm this, we measured the power dependence as shown in Fig. 6(a). The spectrally integrated intensity in the range of the group D peaks sublinearly increased with power. The power dependence was similar to that of the PL intensity of the orthoexciton quadrupole line [indicated

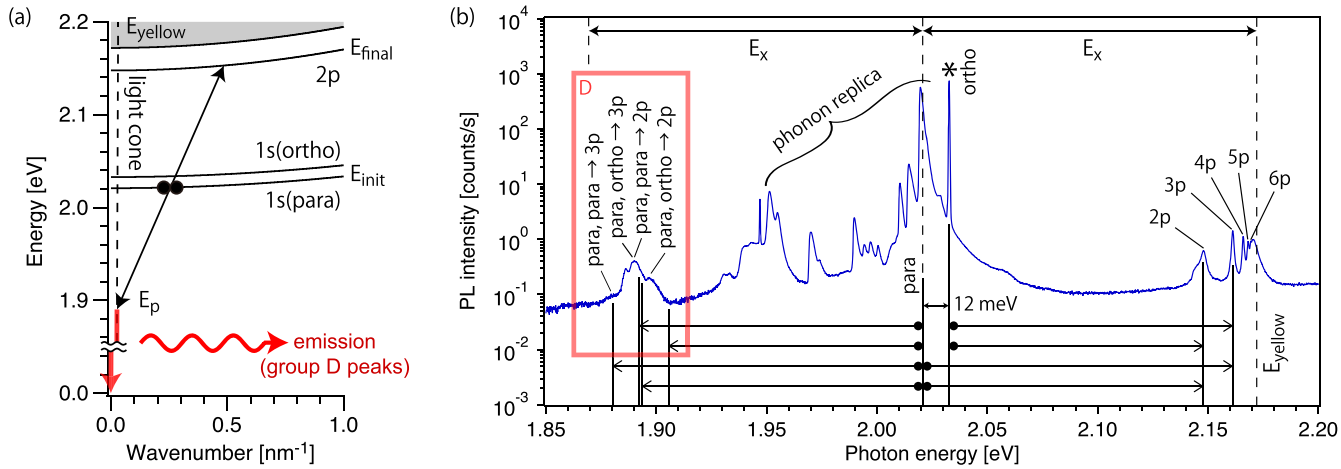

FIG. 5. (a) Schematic of the emissions associated with up-conversion from the 1s paraexcitons to the 2p state. (b) PL spectrum in the region of yellow excitons at 6 K. The horizontal arrows indicate the transfer energies.

by the asterisk symbol in Fig. 5(b)]. In Fig. 6(b), we plotted the integrated intensity as a function of the square root of the orthoexciton intensity. For a good S/N ratio, we used the orthoexciton signal instead of the paraexciton signal, which is weaker by an order of magnitude. Known as the "quantum saturation effect," the paraexciton density changes proportionally with the square root of orthoexciton intensity under continuous-wave excitation. Therefore, the horizontal axis indicates the paraexciton density in a relative unit. We found that the integrated intensity varies proportionally to the squared paraexciton density as indicated by the dashed line. This clearly supports the collision of two paraexcitons as a source for the P-band emission.

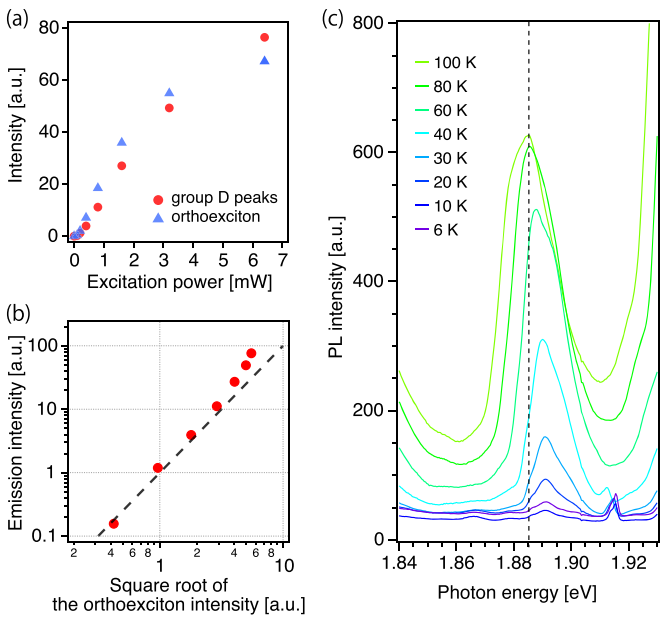

FIG. 6. (a) Intensities of the group D peaks and of the 1s orthoexciton quadrupole line as a function of excitation power. (b) Log-log plot of the emission intensity vs the square root of the orthoexciton intensity. (c) Spectra of the group D peaks obtained at various temperatures.

We should note that the linewidth of the P-band emission is relatively broad owing to the thermal distribution of the excitons in the initial state. Further broadening can be seen in the spectra obtained at increased temperatures as shown in Fig. 6(c). The peak position slightly moves towards the low-energy side with increasing temperature. The line broadening was approximately 12 meV from 6 to 100 K. This width corresponds to an effective temperature of ~140 K, which is on the same order of magnitude as the lattice temperature.

Finally, we would like to emphasize that appearance of the emission lines associated with inelastic collision of the 1s excitons implies formation of the 2p and 3p yellow excitons because these are collision counterparts. Therefore, the present results clearly support our proposal [14] on the formation of high Rydberg yellow excitons via the exciton-exciton collision in the 1s states.

IV. CONCLUSION

We observed the PL spectra in high-quality natural Cu_2O in a wide spectral range under photoexcitation at 3.05 eV. We extracted accurate energy positions and radiative/nonradiative widths of the blue excitons. The temperature variation indicated contributions of acoustic and optical phonon scatterings for the exciton relaxation mechanism. In contrast to the absorption spectra affected by Fano interference with the phonon-assisted transitions, the PL spectra showed clear exciton peaks without background signals and thus served as a particularly powerful tool to provide rich information on the s, p, d, and f states. Despite the successful observations of the PL peaks of violet, blue, and yellow excitons, the PL of the green exciton was not observed. This result indicates that relaxation of holes in the valence band is faster than relaxation of electrons in the conduction band and radiative recombination of the green excitons but is slower than radiative recombination of the violet excitons. We attributed the peaks at the low-energy side of the phonon-assisted 1s yellow lines to the emissions (the so-called P-band emission) associated with inelastic collision of the 1s excitons, based on their energy positions, power dependence, linewidths, and the temperature dependence. The appearance of this emission

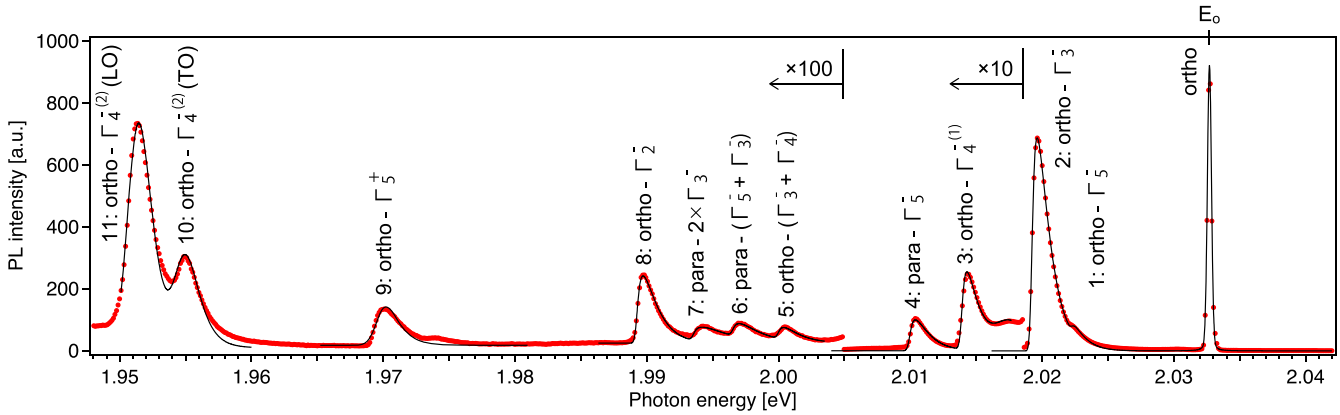

FIG. 7. Phonon-assisted luminescence of ortho- and paraexcitons of the 1*s* yellow state in Cu_2O at 6 K. The black lines represent the fitting results obtained by using the spectral function given by Eq. (A1).

band indicates up-conversion of excitons from the 1*s* states to the *np* states as collision counterparts.

A deep understanding of the properties of excitons in Cu_2O will aid researchers who are interested in the formation of a stable excitonic Bose-Einstein condensate, vast applications of giant Rydberg excitons or atoms, and developments of inexpensive solar cells and catalysts [34]. Furthermore, intra-/interseries exciton relaxation and up-conversion of ground-state excitons can occur in a wide range of materials, and our discussions using a textbooklike semiconductor should stimulate further experimental progress in other materials. Recently, a theory [35] has claimed that the radiative rate of a giant Rydberg exciton increases with the principal quantum number according to an extension of the coherent wave function as opposed to a decrease in the oscillator strength. A breakdown of the long-wavelength approximation and a necessity of quantization of the exciton center-of-mass motion are also pointed out for Rydberg excitons with giant Bohr radii [47]. We hope that our experimental results would help to examine these conceptually novel regimes on the optical properties of Rydberg excitons.

TABLE II. Energy positions of the phonon-assisted lines, measured from the resonance energy of the 1*s* yellow orthoexciton E_o and assignments in the present and previous papers. The errors shown are based on the fitting errors.

Label	E_o-E_i (meV)	Previous paper [31]	Present paper
1	10.51 ± 0.05	Ortho-Γ_5^-	Ortho-Γ_5^-
2	13.52 ± 0.01	Ortho-Γ_3^-	Ortho-Γ_3^-
3	18.84 ± 0.01	Ortho-Γ_4^-	Ortho-$\Gamma_4^{-(1)}$(TO)
4	22.76 ± 0.02	Para-Γ_5^-	Para-Γ_5^-
5	32.78 ± 0.04		Ortho-(Γ_3^-+$\Gamma_4^{-(1)}$(LO))
6	36.24 ± 0.04	Ortho-($2 \times \Gamma_3^-$+Γ_5^-)	Para-(Γ_3^-+Γ_5^-)
7	39.25 ± 0.03	Ortho-$3 \times \Gamma_3^-$	Para-$2 \times \Gamma_3^-$
8	43.49 ± 0.01	Ortho-Γ_2^-	Ortho-Γ_2^-
9	63.20 ± 0.02	Ortho-Γ_5^+	Ortho-Γ_5^+
10	78.42 ± 0.02	Ortho-Γ_4^-(TO)	Ortho-$\Gamma_4^{-(2)}$(TO)
11	82.02 ± 0.01	Ortho-Γ_4^-(LO)	Ortho-$\Gamma_4^{-(2)}$(LO)

ACKNOWLEDGMENTS

We thank Y. Furukawa and M. Mori (Kyoto University) for their valuable contributions in building the high-resolution spectroscopy setup and Y. Kubo (Kyoto University) for his helpful advice on chemical etching. This work was partially supported by a Grant-in-Aid for Scientific Research (C) (Grant No. 26400317) and a Grant-in-Aid for Scientific Research (B) (Grant No. 17H02910) from JSPS, Japan.

APPENDIX: ASSIGNMENT OF THE PHONON-ASSISTED LINES

Figure 7 shows an enlarged spectrum for the region within Box C. Except for the quadrupole line of the 1*s* yellow orthoexcitons at $E_o = 2.032\,70$ eV (at 6 K), all the phonon-assisted lines exhibit asymmetric shapes with tails into the high-energy side. We analyzed the spectral shapes by assuming a Maxwell-Boltzmann distribution,

$$I(E) \propto \sqrt{E - E_i}\,\exp[-(E - E_i)/(k_B T_{\rm eff})], \qquad \text{(A1)}$$

of excitons at an effective temperature of $T_{\rm eff} = 9$ K. We fit the spectra with a spectral function convoluted with a Gaussian representing the spectral resolution of the detection system and adjusted the position of the edge E_i. The obtained energies E_i ($i = 1, 2, \ldots, 11$) and assignments of the peaks are shown in Table II.

TABLE III. Comparison of phonon energies (in units of meV) obtained in previous and present papers.

Phonon	Previous paper [31]	Present paper
Γ_5^-	10.8	10.5
Γ_3^-	13.6	13.5
$\Gamma_4^{-(1)}$(TO)	18.8	18.8
$\Gamma_4^{-(1)}$(LO)	19.1	19.3
Γ_2^-	43.4	43.5
Γ_5^+	63.9	63.2
$\Gamma_4^{-(2)}$(TO)	78.5	78.4
$\Gamma_4^{-(2)}$(LO)	82.1	82.0

Compared to previous reports [31], we obtained one new attribution for line 5 to the $(\Gamma_3^- + \Gamma_4^{-(1)}(\mathrm{LO}))$ phonon-assisted transition of the orthoexciton and two different attributions for lines 6 and 7: the $(\Gamma_3^- + \Gamma_5^-)$ line of the paraexciton instead of the $(2 \times \Gamma_3^- + \Gamma_5^-)$ line of the orthoexciton, and the $2 \times \Gamma_3^-$ line of the paraexciton instead of the $3 \times \Gamma_3^-$ line of the orthoexciton. The latter two lines are reported also in Ref. [53]. These transitions, involving two odd-parity phonons, are forbidden if the parity is conserved. This might be the reason that these assignments were excluded in the past reports [31]. Nevertheless, our spectral resolution of 0.89 meV clearly differentiates the ortho-para-separation of 12.2 meV and the Γ_3^- phonon energy of 13.5 meV. Similarly, not satisfying the parity conservation, single even-parity (Γ_5^+) phonon-assisted transition of the orthoexciton was also observed. These transitions are favored by large momentum excitons as pointed out in Ref. [53].

After the assignments of the phonon-assisted lines, we obtained the energies of each phonon. The results are summarized in Table III.

[1] D. W. Snoke, A. J. Shileds, and M. Cardona, Phonon-absorption recombination luminescence of room-temperature excitons in Cu_2O, Phys. Rev. B **45**, 11693 (1992).

[2] C. Klingshirn, J. Fallert, H. Zhou, J. Sartor, C. Thiele, F. Maier-Flaig, D. Schneider, and H. Kalt, 65 years of ZnO research - old and very recent results, Phys. Status Solidi B **247**, 1424 (2010).

[3] R. Ishii, A. Kaneta, M. Funato, and Y. Kawakami, All deformation potentials in GaN determined by reflectance spectroscopy under uniaxial stress: Definite breakdown of the quasicubic approximation, Phys. Rev. B **81**, 155202 (2010).

[4] R. Ishii, M. Funato, and Y. Kawakami, Huge electron-hole exhange interaction in alminum nitride, Phys. Rev. B **87**, 161204(R) (2013).

[5] G. Wang, A. Chernikov, M. M. Glazov, T. F. Heinz, X. Marie, T. Amand, and B. Urbaszek, Colloquium: Excitons in atomically thin transition metal dichalcogenides, Rev. Mod. Phys. **90**, 021001 (2018).

[6] C. Klingshirn and H. Haug, Optical properties of highly exited firect gap semiconductors, Phys. Rep. **70**, 315 (1981).

[7] F. Mahmood, Z. Alpichshev, Y.-H. Lee, J. Kong, and N. Gedik, Observation of exciton-exciton interaction mediated valley depolarization in monolayer $MoSe_2$, Nano Lett. **18**, 223 (2018).

[8] E. Gross, S. Permogorov, V. Travnikov, A. Selkin, Hot excitons and exciton excitation spectra, J. Phys. Chem. Solids **31**, 2595 (1970).

[9] M. Sugisaki, M. Nishikawa, O. Arimoto, K. Nakamura, K. Tanaka, and T. Suemoto, Emission from the higher members of exciton ($n = 2$, 3 and 4) in β–ZnP_2, J. Phys. Soc. Jpn. **64**, 3506 (1995).

[10] E. Tokunaga, A. L. Ivanov, S. V. Nair, and Y. Masumoto, Inverse exciton series in the optical decay of an excitonic molecule, Phys. Rev. B **59**, R7837(R) (1999).

[11] A. Chernikov, M. Koch, B. Laumer, T. A. Wassner, M. Eickhoff, S. W. Koch, and S. Chatterjee, Intra-excitonic relaxation dynamics in ZnO, Appl. Phys. Lett. **99**, 231910 (2011).

[12] A. Compaan and H. Z. Cummins, Raman Scattering, Luminescence, and exciton-phonon coupling in Cu_2O, Phys. Rev. B **6**, 4753 (1972).

[13] M. Manca, M. M. Glazov, C. Robert, F. Cadiz, T. Taniguchi, K. Watanabe, E. Courtade, T. Amand, P. Renucci, X. Marie, G. Wang, and B. Urbaszek, Enabling valley selective exciton scattering in monolayer WSe_2 through upconversion, Nat. Commun. **8**, 14927 (2016).

[14] T. Kitamura, M. Takahata, and N. Naka, Quantum number dependence of the photoluminescence broadening of excitonic Rydberg states in cuprous oxide, J. Lumin. **192**, 808 (2017).

[15] E. F. Gross and N. A. Karryev, Opticheskii spektr eksitona, Dokl. Akad. Nauk. SSSR **84**, 471 (1952).

[16] D. W. Snoke and G. M. Kavoulakis, Bose-Einstein condensation of excitons in Cu_2O: Progress over thirty years, Rep. Prog. Phys. **77**, 116501 (2014).

[17] K. Yoshioka, Y. Morita, K. Fukuoka, and M. Kuwata-Gonokami, Generation of ultracold paraexcitons in cuprous oxide: A path toward a stable Bose-Einstein condensate, Phys. Rev. B **88**, 041201(R) (2013).

[18] T. Kazimierczuk, D. Fröhlich, S. Scheel, H. Stolz, and M. Bayer, Giant Rydberg excitons in the copper oxide Cu_2O, Nature (London) **514**, 343 (2014).

[19] J. Heckötter, M. Freitag, D. Fröhlich, M. Assmann, M. Bayer, M. A. Semina, and M. M. Glazov, High-resolution study of the yellow excitons in Cu_2O subject to an electric field, Phys. Rev. B **95**, 035210 (2017).

[20] F. Schweiner, J. Main, and G. Wunner, Magnetoexitons in cuprous oxide, Phys. Rev. B **95**, 035202 (2017).

[21] M. Kurz, P. Grünwald, and S. Scheel, Excitonic giant-dipole potentials in cuprous oxide, Phys. Rev. B **95**, 245205 (2017).

[22] S. Artyukhin, D. Fishman, C. Faugeras, M. Potemski, A. Revcolevscki, M. Mostovoy, and P. H. M. van Loosdrecht, Magneto-absorption spectra of hydrogen-like yellow exciton series in cuprous oxide: Excitons in strong magnetic fields, Sci. Rep. **8**, 7818 (2018).

[23] S. Zielińska-Raczyńska, D. Ziemkiewicz, and G. Czajkowski, Electro-optical properties of Cu_2O for P excitons in the regime of Franz-Keldysh oscillations, Phys. Rev. B **97**, 165205 (2018).

[24] M. Assmann, J. Thewes, D. Fröhlich, and M. Bayer, Quantum chaos and breaking of all anti-unitary symmetries in Rydberg excitons, Nature Mater. **15**, 741 (2016).

[25] P. Grünwald, M. Assmann, J. Heckötter, D. Fröhlich, M. Bayer, H. Stolz, and S. Scheel, Signatures of Quantum Coherences in Rydberg Excitons, Phys. Rev. Lett. **117**, 133003 (2016).

[26] S. Brahms and S. Nikitine, Intrinsic absorption and reflection of cuprous oxide in the 2.5 to 6.5 eV region, Solid State Commun. **3**, 209 (1965).

[27] A. Daunois, J. L. Deiss, and B. Mayer, Etude spectrophotometrique de labsorption bleue et violette de Cu_2O, J. Phys. **27**, 142 (1966).

[28] S. N. Shestatskii, V. V. Sobolev, and N. P. Likhobabin, Exciton electro-reflectance of cuprous oxide crystals, Phys. Status Solidi B **42**, 669 (1970).

[29] K. C. Rustagi, F. Pradere, and A. Mysyrowicz, Two-photon absorption in Cu_2O, Phys. Rev. B **8**, 2721 (1973).

[30] N. Naka and N. Nagasawa, Dynamics of paraexcitons generated in a 3D confined potential well by two-photon resinance excitation in Cu_2O, J. Lumin. **94-95**, 413 (2001).
[31] Y. Petroff, P. Y. Yu, and Y. R. Shen, Study of photoluminescence in Cu_2O, Phys. Rev. B **12**, 2488 (1975).
[32] K. Reimann and K. Syassen, Ramand scattering and photoluminescence in Cu_2O under hydrostatic pressure, Phys. Rev. B **39**, 11113 (1989).
[33] E. F. Gross, Optical spectrum of excitons in the crystal lattice, Riv. Nuovo Cimento **S3**, 672 (1956).
[34] B. K. Meyer, A. Polity, D. Reppin, M. Becker, P. Hering, P. J. Klar, T. Sander, C. Reindl, J. Benz, M. Eickhoff, C. Heiliger, M. Heinemann, J. Bläsing, A. Krost, S. Shokovets, C. Müller, and C. Ronning, Binary copper oxide semiconductors: From materials towards devices, Phys. Status Solidi B **249**, 1487 (2012).
[35] H. Stolz, F. Schöne, and D. Semkat, Interaction of Rydberg excitons in cuprous oxide with phonons and photons: Optical linewidth and polariton effect, New J. Phys. **20**, 023019 (2018).
[36] I. Pelant and J. Valenta, *Luminescence Spectroscopy of Semiconductors* (Oxford University Press, Oxford, 2012), p. 83.
[37] M. Takahata, K. Tanaka, and N. Naka, Nonlocal optical response of weakly confined excitons in Cu_2O mesoscopic films, Phys. Rev. B **97**, 205305 (2018).
[38] M. M. Beg and S. M. Shapiro, Study of phonon dispersion relations in cuprous oxide by inelastic neutron scattering, Phys. Rev. B **13**, 1728 (1976).
[39] C. Carabatos and B. Prevot, Rigid ion model lattice dynamics of cuprite (Cu_2O), Phys. Status Solidi B **44**, 701 (1971).
[40] S. Rudin, T. L. Reinecke, and B. Segall, Temperature-dependent exciton linewidth in semiconductors, Phys. Rev. B **42**, 11218 (1990).
[41] S. Rudin and T. L. Reinecke, Effects of exciton-acoustic phonon scattering on optical line shapes and exciton dephasing in semiconductors and semicondutor quantum wells, Phys. Rev. B **66**, 085314 (2002).
[42] A. V. Gopal, R. Kumar, A. S. Vengurlakar, A. Bosacchi, S. Franchi, and L. N. Pfeiffer, Photoluminescence study of exciton-optical phonon scattering in bulk GaAs and GaAs quantum wells, J. Appl. Phys. **87**, 1858 (2000).
[43] C. W. Chang, H. C. Yang, C. H. Chen, H. J. Chang, and Y. F. Chen, Optoelectronic properties of ZnSe/ZnMgSSe multiple quantum wells, J. Appl. Phys. **89**, 3725 (2001).
[44] C. Uihlein, D. Fröhlich, and R. Kenklies, Investigation of exciton fine structure in Cu_2O, Phys. Rev. B **23**, 2731 (1981).
[45] N. Naka, I. Akimoto, and M. Shirai, Free-carrier generation by two-photon resonant excitation to the excitonic states in cuprous oxide, Phys. Status Solidi B **250**, 1773 (2013).
[46] J. Thewes, J. Heckötter, T. Kazimierczuk, M. Assmann, D. Fröhlich, M. Bayer, M. A. Semina, and M. M. Glazov, Observation of High Angular Momentum Excitons in Cuprous Oxide, Phys. Rev. Lett. **115**, 027402 (2015).
[47] S. Zielinska-Raczynska, D. Ziemkiewicz, and G. Czajkowski, Magneto-optical properties of Rydberg excitons: Center-of-mass quantization approach, Phys. Rev. B **95**, 075204 (2017).
[48] F. Schweiner, J. Main, G. Wunner, and C. Uihlein, Even exciton series in Cu_2O, Phys. Rev. B **95**, 195201 (2017).
[49] F. Schöne and H. Stolz (private communication).
[50] M. Bamba, S. Wakaiki, H. Ichida, K. Mizoguchi, D. G. Kim, M. Nakayama, and Y. Kanematsu, Theory of the lifetime of an exciton incoherently created below its resonance frequency by inelastic scattering, Phys. Rev. B **91**, 235205 (2015).
[51] C. Benoit a la Guillaume, J. M. Debever, and F. Salvan, Radiative recombination in highly excited CdS, Phys. Rev. **177**, 567 (1969).
[52] K. E. O'Hara, J. R. Gullingsrud, and J. P. Wolfe, Auger decay of excitons in Cu_2O, Phys. Rev. B **60**, 10872 (1999).
[53] C. Sandfort, J. Brandt, D. Fröhlich, M. Bayer, and H. Stolz, Resonant phonon scattering of paraexcitons in Cu_2O, Phys. Rev. B **78**, 045201 (2008).